6-2019

Monolayer triphosphates MP_3 (M = Sn, Ge) with excellent basal catalytic activity for hydrogen evolution reaction

Hong-Hui Wu
University of Nebraska - Lincoln, honghui.wu@unl.edu

He Huang
Hong Kong University of Science and Technology

Jie Zhong
University of Nebraska–Lincoln, jzhong4@unl.edu

Song Yu
East China Normal University

Qiaobao Zhang
Xiamen University, zhangqiaobao@xmu.edu.cn

See next page for additional authors

Monolayer triphosphates MP_3 (M = Sn, Ge) with excellent basal catalytic activity for hydrogen evolution reaction

Hong-Hui Wu,[2] He Huang,[3] Jie Zhong,[2] Song Yu,[4] Qiaobao Zhang,[1] and Xiao Cheng Zeng[2]

1 Department of Materials Science and Engineering, College of Materials, Xiamen University, Xiamen, Fujian 361005, China
2 Department of Chemistry, University of Nebraska-Lincoln, Lincoln, NE 68588, USA
3 Department of Mechanical and Aerospace Engineering, Hong Kong University of Science and Technology, Clear Water Bay, Kowloon, Hong Kong, China
4 Department of Physics and Materials, East China Normal University, Shanghai 200241, China

Corresponding authors — Qiaobao Zhang, *email* zhangqiaobao@xmu.edu.cn ; Xiao Cheng Zeng, *email* xzeng1@unl.edu

ORCIDs:

Hong-Hui Wu http://orcid.org/0000-0002-1381-2281
Qiaobao Zhang http://orcid.org/0000-0002-3584-5201
Xiao Cheng Zeng http://orcid.org/0000-0003-4672-8585

Published in *Nanoscale* 11 (2019), 12210
DOI: 10.1039/c9nr03255j

Submitted 16th April 2019; accepted 7th June 2019.
† ESI/SI: Electronic supplementary information available at doi 10.1039/c9nr03255j ; Supplementary information also available following the **References**.

Abstract

Atomically thin two-dimensional (2D) materials have received intense research interest due to their novel properties and promising applications in nanodevices. By using density functional theory (DFT) calculations, we investigate catalytic activities of several newly predicted two-dimensional (2D) triphosphides GeP_3, SnP_3 and InP_3 monolayers for hydrogen evolution reaction (HER). The calculation results show that GeP_3 and SnP_3 monolayers are active catalysts for HER with suitable free energy of hydrogen adsorption in the basal plane. In particular, the Gibbs free energy of hydrogen adsorption (ΔG_{H^*}) of GeP_3 is 0.024 eV, a value even more favorable compared to the precious-group-metal (PGM) catalyst Pt. Moreover, the 2D GeP_3 and SnP_3 are intrinsically compatible with the graphene substrate so that the HER performance can be improved via building a hybrid multilayer with graphene sheet. The charge transfer from GeP_3 or SnP_3 to graphene, estimated to be 0.1278e or 0.2157e, can significantly enhance the electric conductivity and promote the electrocatalytic activity. Although the electronic band structure of GeP_3 and SnP_3 can be tuned by external strain, we find that the HER performance of GeP_3 and SnP_3 monolayer is actually insensitive to the external strain, a feature desirable for the catalytic application. The desirable properties for HER with nearly zero Gibbs free energy render 2D GeP_3 and SnP_3 promising candidates for future application in electrocatalysis.

1. Introduction

Since the discovery of graphene,[1–3] two-dimensional (2D) monolayer nanomaterials have received considerable attention owing to their rich physical phenomena, novel properties, and promising applications in nanoscale devices.[4–8] Beyond graphene, many 2D materials have been predicted and fabricated, such as silicene,[9] phosphorus allotropes,[10] MXenes,[11] and transition-metal chalcogenides,[12] among many others. To date, potential applications of 2D materials in field-effect transistors,[13,14] batteries,[15] light-emitting devices,[16] photovoltaic solar cells,[17] and photocatalysts[18] have been studied extensively.[19] Among them, 2D triphosphides, a new class of 2D materials, have attracted growing attention in recent years. Their monolayer structures are closely related to that of arsenic, which can be viewed as replacement of every fourth atom in the arsenic layer by a (Ge, or Sn, In) atom and of the rest by phosphorus (P) atom. Examples in this class of 2D materials include combination of phosphorus with group-II, III, and IV elements, which result in easily exfoliable 2D materials with low cleavage

energies for monolayer, such as calcium triphosphide (CaP_3),[20] indium triphosphide (InP_3),[21] tin triphosphide (SnP_3),[22] and germanium triphosphide (GeP_3).[23] In particular, monolayer GeP_3[23] was theoretically predicted to be a novel 2D structure with tunable indirect bandgaps, high carrier mobilities, and an excellent absorption coefficient in the range of solar spectrum, and it can be easily exfoliated from GeP_3 bulk material. It is also predicted that SnP_3[22] monolayer exhibits high carrier mobility and tunable band gap by strain engineering.

2D MP_3 (X = Ge, Sn, In) have also been suggested as high capacity electrode material for Li-ion batteries due in part to their novel properties predicted.[24,25] Zhang *et al.*[24] investigated the adsorption and diffusion of Li on the 2D GeP_3 monolayer by using density functional theory (DFT) calculations. They estimated the capacity of 648 mA h g^{-1}, about twice of that of commercially used graphite (375 mA h g^{-1}), and they also predicted semiconductor to metal transition, induced by Li adsorption. Liu and co-workers[25] theoretically predicted the SnP_3 monolayer with an ultralow energy barrier (0.03 eV) for Na diffusion. However, the reported band gaps of GeP_3 (0.55 eV),[23] SnP_3 (0.72 eV),[22,26] and InP_3 (1.14 eV)[21] monolayers are relatively narrow so that they are unsuitable for photocatalysis.

Hydrogen (H_2) is regarded as an ideal and renewable energy carrier because H_2O is the oxidation product. It has high energy capacity of 143 MJ kg^{-1}.[27] Hydrogen produced through electrocatalytic water splitting has been considered as one of the most important sources of future renewable energy. For practical applications, platinum, as the most active catalyst, is needed to facilitate the low overpotential and fast kinetics. However, the high expense and scarcity of PGM platinum (Pt)-based electrocatalysts greatly hamper their wide utilization. Development of highly efficient, earth-abundant, and low-cost alternative catalysts is thus greatly needed. Thus far, extensive efforts have been devoted to such development both experimentally and theoretically.[19]

Electrochemical hydrogen evolution involves hydrogen binding and hydrogen desorption on the catalyst surface. The hydrogen adsorption free energy ΔG_{H^*} is an effective descriptor for the rate of HER with the ideal value of ΔG_{H^*} being 0 eV.[28] An optimal catalyst for HER would be able to bind hydrogen neither too strongly nor too weakly. Ultrathin 2D catalysts would be desirable for electrocatalysis due to

their extremely large surface areas and relatively low cost. Among 2D materials, trilayer MoS_2 was theoretically predicted to be a promising candidate for HER, although MoS_2 nanoparticles and clusters have subsequently also been predicted to be excellent electrocatalysts.[29] However, the large basal plane of MoS_2 has been found, from both experiment and theory, to be chemically inert ($\Delta G_{H^*} > 1.24$ eV),[30,31] and MoS_2's high activity has been attributed to the edges of the MoS_2 sheet or MoS_2 nanoparticles.[31,32] Although many other efforts have been devoted to finding replaceable 2D materials,[33,34] replacing PGM Pt by 2D crystals remains a challenge. In addition, the lattice compatibility with other 2D substrate, *e.g.*, graphene, further limits the available selections.

In this work, we performed a systematic investigation of potential electrocatalytic application of 2D triphosphates SnP_3, GeP_3 and InP_3 for the HER, in view of that the thermal and dynamic stability of SnP_3, GeP_3 and InP_3 have been confirmed *via* the phonon dispersion computation and *ab initio* MD simulation in previous studies.[21–23] First, we examine the adsorption free energy of the three 2D materials. Knowing that the HER related properties and the compatibility with graphene for InP_3 is not so good, we only focus on the other two materials (GeP_3 and SnP_3) and examine their hybrid heterobilayers with graphene substrate for potential application in electrocatalysis. We find that GeP_3 is quite suitable for the electrocatalysis, as the Gibbs free energy of hydrogen adsorption (ΔG_{H^*}) is even more desirable than that of the PGM catalyst, Pt. For the SnP_3 monolayer, the free energy of hydrogen adsorption can be tuned to be about zero, when a compressive strain is imposed. We further explore the influence of the substrate on the HER performance and find that the HER performance of GeP_3@graphene and SnP_3@graphene can be further enhanced. The present study provides important guidance for future development of 2D triphosphides-based materials as PGM-free catalysts.

2. Computational details

The spin-polarized density functional theory (DFT) calculations are carried out using the projector augmented wave (PAW) potentials as implemented in the Vienna *ab initio* Simulation Package (VASP 5.4).[35,36]

Plane-wave basis sets with a kinetic energy cutoff of 520 eV are used. The exchange–correlation energy density functional selected is within the generalized gradient approximation (GGA) in the form of Perdew–Burke–Ernzerhof (PBE) functional.[37,38] The van der Waals (vdW) interaction is described by using the DFT-D3 method for all calculations. The convergence criterion is set to be 10^{-5} eV for the energy and 0.01 eV $Å^{-1}$ for the force, respectively.[39,40] A vacuum at least 20 Å along the out-plane direction and/or vertical to the nanoribbon edge direction is adopted so that the interaction between periodic units can be neglected. The reciprocal space is sampled on the Gamma centered meshes of 3 × 3 × 1 supercell, ensuring a density larger than 10 $Å^{-1}$. The chemical stability of the GeP_3 and SnP_3 monolayer in presence of water is examined by using the *ab initio* molecular dynamics (AIMD) simulations in the constant-temperature and constant-volume ensemble.[41] The temperature is controlled at 300 K. The time step is set as 1 fs and each simulation lasts 6 ps. Since the semi-local GGA-PBE functional underestimates the band gaps of 2D triphosphide,[21–23,42] the Heyd–Scuseria–Ernzerhof (HSE06) screened hybrid functional[43] with a mixing parameter (α) of default value is also employed to calculate the electronic structures, *e.g.*, the density of state (DOS). The adsorption energy for an H atom on the MP_3 (M = Ge, Sn) sheet is given by

$$\Delta_{EH^*} = E_{MP_3+H} - E_{MP_3} - \tfrac{1}{2}E_{H_2} \quad (1)$$

where E_{MP_3+H} and E_{MP_3} are the energy of the system with and without the adsorption of a hydrogen atom, respectively, and E_{H_2} is the energy of a hydrogen molecule.

The HER catalytic activity for the materials considered can be evaluated by the hydrogen adsorption free energy,[28,44] which is defined as,

$$\Delta G_{H^*} = \Delta E_{H^*} - T\Delta S_H + \Delta E_{ZPE} \quad (2)$$

where ΔE_{H^*} is the hydrogen adsorption energy, ΔE_{ZPE} and ΔS_H are the zero-point energy and the entropy differences between the adsorbed state and gas phase, respectively, and T is the temperature. The contributions from GeP_3 and SnP_3 to both ΔS_H and ΔE_{ZPE} are very small and negligible. So $\Delta S_H = -\tfrac{1}{2}S_{H_2}$, where S_{H_2} is the entropy of a H_2 molecule in the gas phase at standard condition. At 298.15 K, $T\Delta S_H$ is a

constant, about –0.20 eV.[45] ΔE_{ZPE} of the SnP_3, GeP_3 and InP_3 system is obtained from the zero-point energy calculation (~0.21 eV). Therefore, equation (2) can be rewritten as

$$\Delta G_{H^*} = \Delta E_{H^*} + 0.41 \text{ eV} \quad (3)$$

According to the Sabatier principle, an ideal HER catalytic activity occurs when H binding on the surface of reactive intermediates is thermally neutral, *i.e.*, the reaction Gibbs free energy ΔG_{H^*} of H* adsorption is close to zero.[28,46] Catalysts with positive ΔG_{H^*} will cause relatively slow kinetics of hydrogen adsorption, whereas catalysts with negative ΔG_{H^*} indicate the kinetics of H_2 release are relatively low.

3. Results and discussion

Bulk GeP_3 and SnP_3 ($R\bar{3}m$ space group) are layered structures with interlayer van der Waals interaction.[47–49] In monolayers, every Ge (Sn) atom is bonded with three neighboring P atoms, while each P atom forms one Ge–P (Sn–P) bond and two P–P bonds, yielding hexagonal puckered arsenic-type honeycomb configurations. Here, the monolayer GeP_3 and SnP_3 are obtained by a full optimization of a single layer taken from the bulk structure.[21–23] The optimized lattice parameters of monolayer GeP_3 and SnP_3 are $a = b = 6.953$ Å, and $a = b = 7.149$ Å, respectively, consistent with the previous reports.[21,23] As shown in Fig. 1a and b, the Ge (Sn) atoms are located at the outmost atomic layer, while the P atoms are in the middle atomic layer. The computed bond length, thickness, and layer distance are shown in the ESI/SI Table S1.† We use the 9 × 9 × 1 supercell of graphene, and the 3 × 3 × 1 supercell of MP_3, which yield a misfit strain of –0.58%@5.56% and –0.28%@3.21% in the GeP_3@graphene and SnP_3@graphene, respectively. Additionally, after full relaxation, the phosphorus six-atom ring is perfectly corresponding to the carbon six-atom ring in terms of structural match. We calculate the formation energy of MP_3 materials with graphene based on the equation,

$$E_{form} = E_{MP3@graphene} - E_{MP3} - E_{graphene}$$

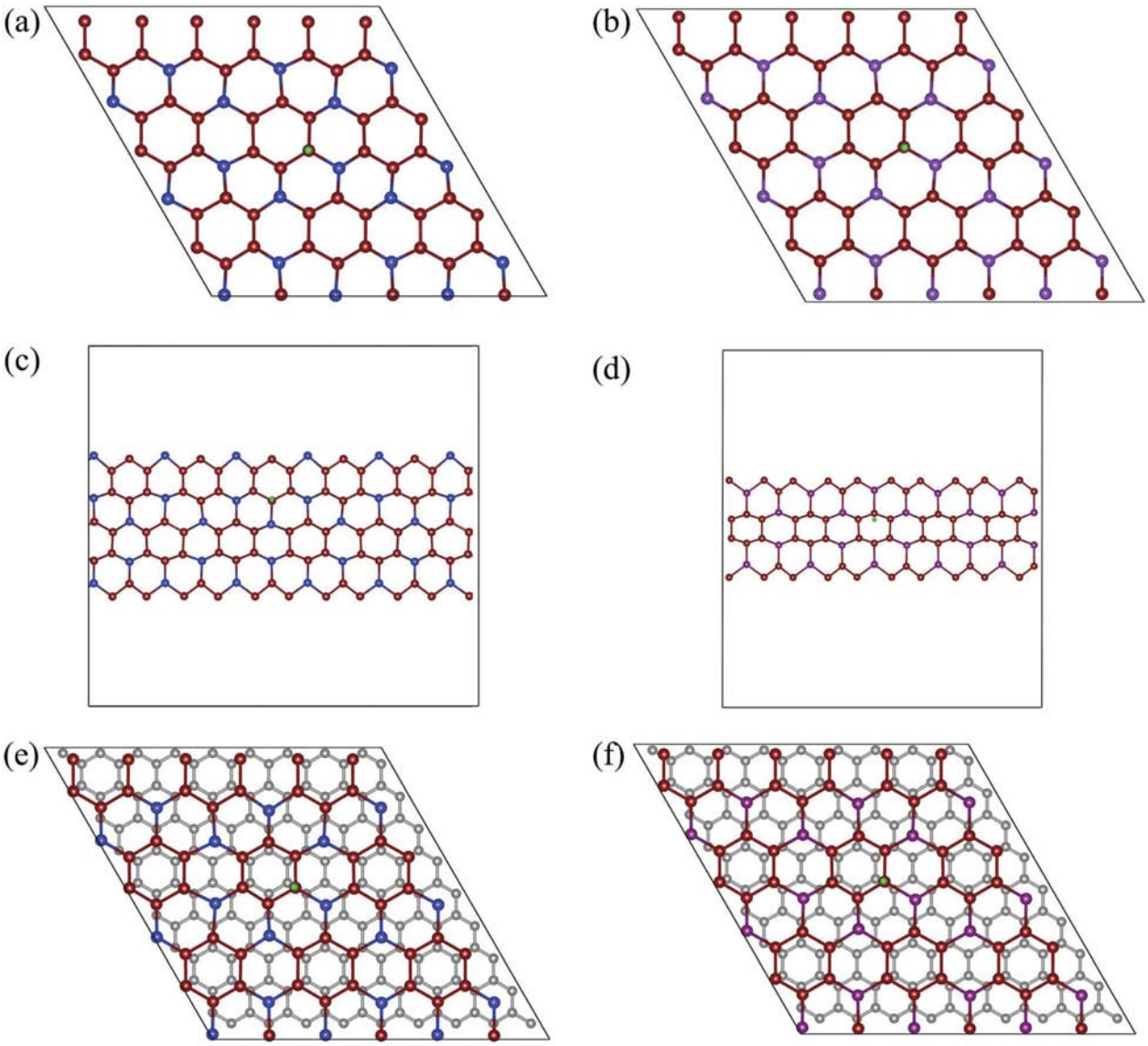

Fig. 1. A favorable H adsorption structures of (a) GeP_3, (b) SnP_3, (c) GeP_3 nanoribbon, (d) SnP_3 nanoribbon, (d) GeP_3@graphene, and (e) SnP_3@graphene. The dark red, blue, purple, and green spheres represent P, Ge, Sn, and H atoms, respectively. Carbon atoms are in grey.

where $E_{MP3@graphene}$, $E_{MP}3$ and $E_{graphene}$ are the energy of MP_3@graphene heterobilayer, MP_3, and graphene, respectively. The formation energy of GeP_3@graphene is –1.232 eV, and the formation energy of SnP_3@graphene is –3.197 eV. The negative value of formation energy indicates the energetic preference of the formation of GeP_3@graphene and SnP_3@graphene heterobilayers. The optimized GeP_3@graphene

and SnP_3@graphene heterobilayers are shown in Fig. 1(e) and (f), respectively. On either GeP_3 or SnP_3 monolayer, three possible sites for H adsorption are labeled as S1, S2 and S3, respectively (see ESI/SI Fig. S1†). The calculated H adsorption energy at the three sites are –0.386, –0.353, 0.038 eV for GeP_3, and –0.137, 0.326, 0.349 eV for SnP_3, respectively. The H adsorption energy of the GeP_3@graphene and SnP_3@graphene heterobilayers are also shown in ESI/SI Fig. S1.† Therefore, the most stable H-adsorption site is the S1 site on which an H–P bond is formed through hybridized H 1s orbital and P $2p_z$ orbital.

Strain engineering has been proven to be an effective way to tune the physical and chemical properties of 2D materials,[50] as well as HER performance.[30,45] Hence, the effect of biaxial strain on the electric properties of GeP_3 and SnP_3 monolayer, with or without a graphene substrate, is also investigated. Fig. 2(a) and (b) presents the

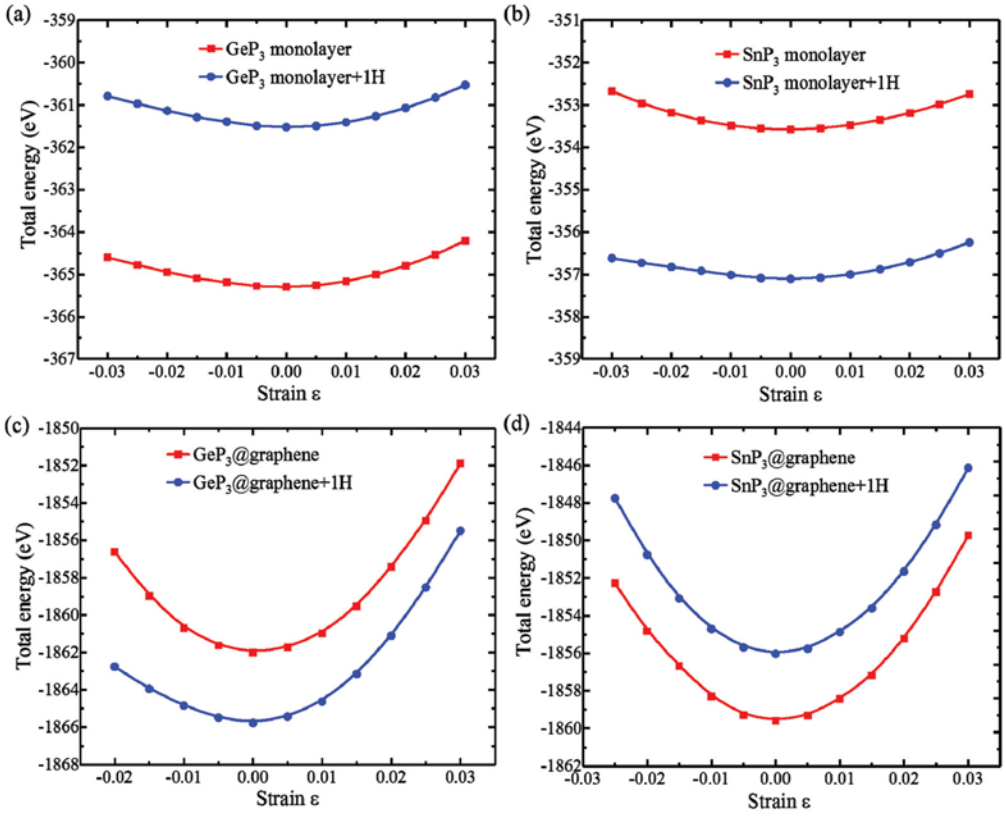

Fig. 2. Total energy versus the biaxial strain for (a) GeP_3 monolayer with and without adsorption of an H atom, (b) SnP_3 monolayer with and without adsorption of an H atom, (c) GeP_3@graphene heterobilayer with and without adsorption of an H atom, (d) SnP_3@graphene heterobilayer with and without adsorption of an H atom.

biaxial strain effect on the total energy of the GeP_3 and SnP_3 monolayer with and without H adsorption, respectively. The applied mechanical strain ε is defined as $\varepsilon = \Delta l/l_0$, where l_0 is the equilibrium lattice constant and Δl is the change of the lattice constant. We can see that all the energy shows a quadratic dependence on the applied biaxial strain, and there is no mutation in the curves, indicating that the systems are within the elastic strain range. The external in-plane strain will increase the total energy for all the simulated systems. For the GeP_3 monolayer shown in Fig. 2a, the total energy changes almost in synchronous fashion for the GeP_3 monolayer with and without an H atom adsorbed. In other words, the energy difference is insensitive to the H adsorption in the studied strain range. The same trend is also seen for the SnP_3 shown in Fig. 2b. However, when GeP_3 or SnP_3 is attached to a graphene substrate, the energy change is no longer in synchronous fashion, for the cases of with and without hydrogen adsorption. Fig. 2(c) and (d) show the variation of total energy *versus* biaxial strain for the GeP_3@graphene and SnP_3@graphene system with and without adsorption of an H atom. Clearly, the energy difference is sensitive to the external strain. Since the adsorption free energy ΔG_{H^*} is proportional to the total energy difference, the adsorption free energies of GeP_3@graphene and SnP_3@graphene system are tunable by the external strain.

In general, the intrinsic catalytic activity of a material for HER can be theoretically characterized by the Gibbs free energy ΔG_{H^*} of hydrogen adsorption. ΔG_{H^*} is a suitable descriptor for the rate of reaction and has been widely used for predicting the HER performance of various materials.[32,33,45] To examine whether monolayer GeP_3, SnP_3 and InP_3 are promising for HER, we first compute the adsorption free energy of an H atom on each of the three monolayer. As shown in Fig. 3, the descriptors suggest that the HER activity of GeP_3 (ΔG_{H^*} = 0.024 eV) without external strain seems superior to that of SnP_3 (ΔG_{H^*} = 0.273 eV). Interestingly, the ΔG_{H^*} value for GeP_3 is very close to that of the perfect HER electrocatalyst (0 eV), and is even closer to 0 eV compared to that of the well-known PGM catalyst Pt (ΔG_{H^*} = –0.167 eV), and much better than that of 2D MoS_2 (measured by ΔG_{H^*} = 1.24 eV for basal plane, and –0.48 eV for etched edge).[31] Note that both catalysts have been proven to show excellent catalytic activity. For InP_3, the relatively high ΔG_{H^*} value of 0.41 eV suggests its weak binding

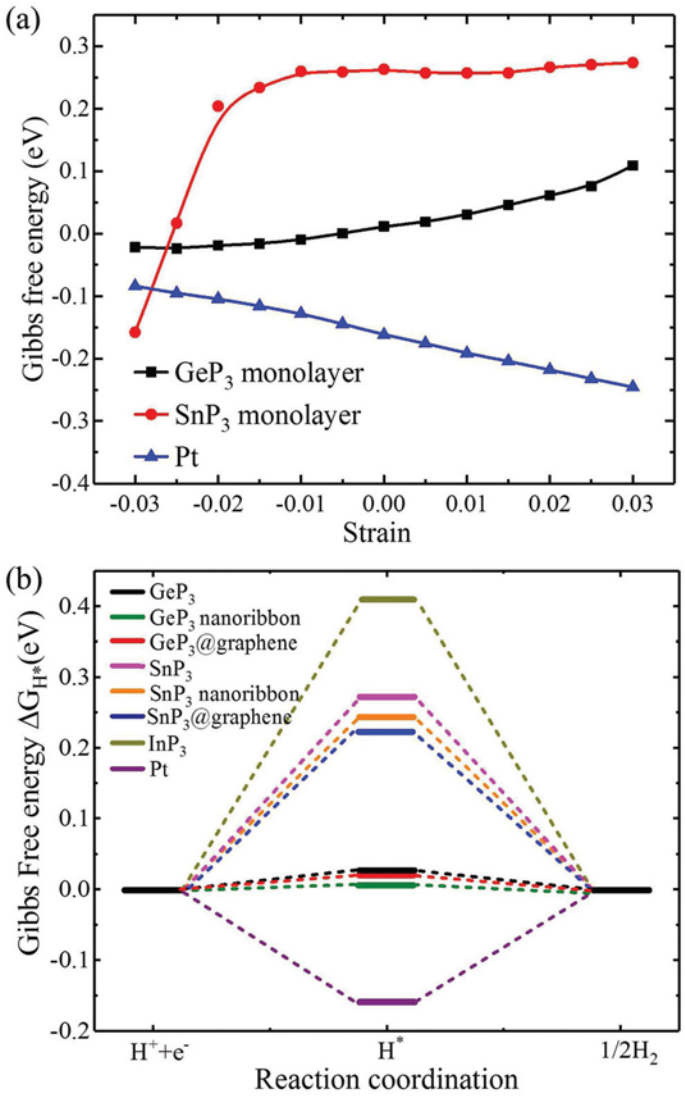

Fig. 3. (a) Computed free energy ΔG_{H^*} versus in-plane biaxial strain, and (b) computed adsorption free energy diagram of hydrogen evolution (including Pt for the comparison).

strength of H atom, which renders H adsorption difficult. Compared with GeP_3 and SnP_3, InP_3 is not a good catalyst for HER.

Interestingly, although previous studies[23] showed that the band gap of 2D GeP_3 is sensitive to the compressive and tensile biaxial in-plane strain, we find that the HER performance of 2D GeP_3 seems insensitive to the external strain, at least for the strain in the range from –0.030 to 0.030. This feature is desirable for practical applications. On

the other hand, the HER performance of 2D SnP_3 seems quite sensitive to the external strain, as the ΔG_{H^*} can be tuned to about zero at a compressive strain of –0.025. These results of HER performance are based on the free-standing GeP_3 and SnP_3 monolayers. In reality, the fabricated 2D materials are usually grown on certain substrates. So the influence of the graphene substrate on the HER activity is also examined. As shown in Fig. 3b, the graphene substrate has a slightly positive effect on the HER performance in that the ΔG_{H^*} of GeP_3@graphene and ΔG_{H^*} of SnP_3@graphene are reduced to 0.021 eV and 0.226 eV, respectively, due to the attachment with the graphene substrate. The decrease of ΔG_{H^*} value can be ascribed to that the interaction between the MP_3 and graphene substrate causes charge transfer from the graphene substrate to the GeP_3 (SnP_3) sheet. Indeed, based on the Bader charge computation, the adsorption site gains 0.032*e* and 0.067*e* more charge than the free-standing GeP_3 and SnP_3 monolayer (see Table S2†), respectively. Overall, it appears that the HER electrocatalytic activity of GeP_3 and SnP_3 monolayer based structures can be more superior to that of popular 2D transition metal dichalcogenides, *e.g.*, MoS_2 and WS_2 monolayers. The edge effect is often used to adjust the HER performance in previous studies. Thus, we consider a nanoribbon model to study the edge effect. It is found that the HER performance of both GeP_3 and SnP_3 nanoribbons is enhanced compared with the corresponding monolayer structures. Other types of defects,[19] *e.g.*, point defect, dislocation *etc.*, can also affect the electrocatalytic performance for HER, which will be considered in our future work. To confirm the chemical stability of the GeP_3 and SnP_3 monolayer in presence of water,[51,52] *ab initio* molecular dynamics (AIMD) simulations are conducted for both GeP_3 and SnP_3 in 6 × 6 × 1 supercell with total 32 water molecules. As shown in ESI/SI Fig. S5 and S6,† both monolayers appear to be intact and are not poisoned/degraded under reaction condition within the timescale of AIMD simulations. So application of GeP_3 and SnP_3 monolayers for HER is likely experimentally achievable.

Fig. 4 shows the computed total density of state (TDOS) and partial density of states (PDOS) of GeP_3, SnP_3 monolayer, GeP_3@graphene and SnP_3@graphene heterobilayers based on the HSE06 calculation. The pristine GeP_3 and SnP_3 monolayers are semiconductors with a band gap of 0.55 eV for GeP_3 and 0.72 eV for SnP_3, consistent with

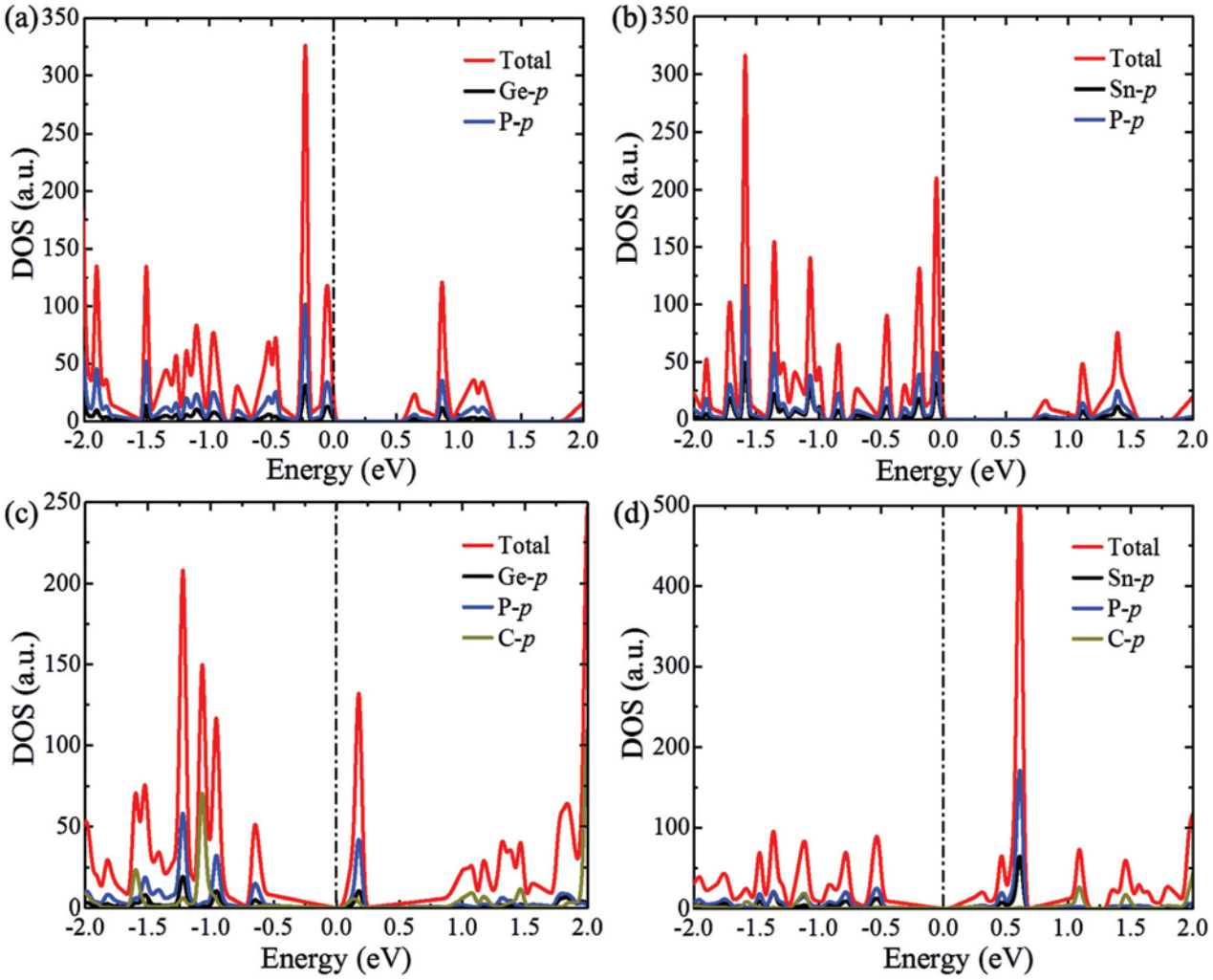

Fig. 4. Total and partial density of states based on the HSE06 calculation for (a) GeP_3 monolayer, (b) SnP_3 monolayer, (c) GeP_3@graphene heterobilayer, (d) SnP_3@graphene heterobilayer.

previous literature.[22,23] As a comparison, the TDOS plots based on PBE calculation are shown in ESI/SI Fig. S2.† One can see that the PBE functional underestimates the band gap by about half of the HSE06 band gap. The effect of in-plane strain on the TDOS of GeP_3 and SnP_3 monolayer are shown in ESI/SI Fig. S3 and S4,† respectively. The results show that the band gap of the GeP_3 and SnP_3 monolayer increases when the strain is changed from compressive to tensile value. For the heterobilayers of GeP_3 and SnP_3 (together with a graphene sheet), the band gap is reduced to 0.066 eV and 0.052 eV, respectively, while the charge transfer from GeP_3 or SnP_3 to graphene is 0.1278*e* or

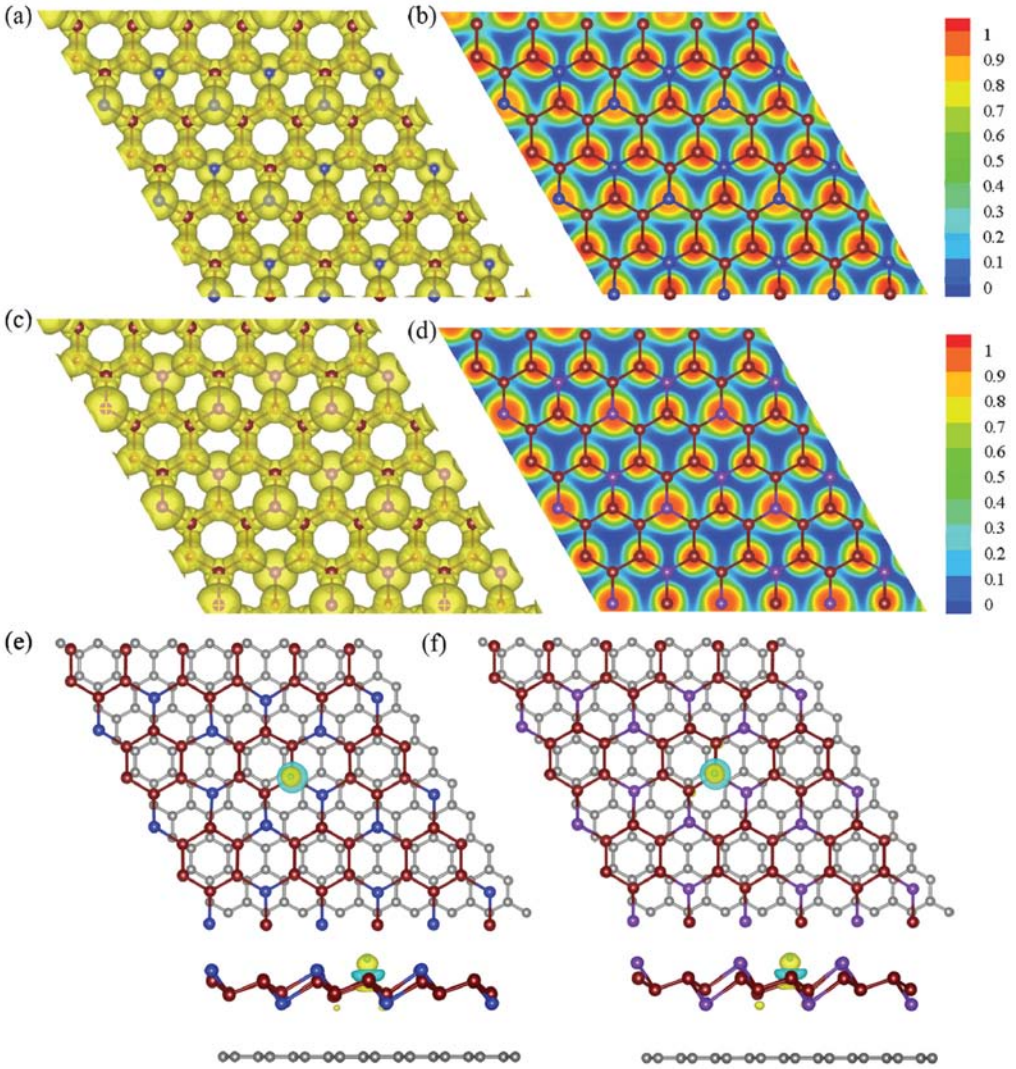

Fig. 5. The electron localization function of (a) 3D and (b) 2D GeP_3 monolayer, (c) 3D and (d) 2D SnP_3 monolayer; and the differential charge density of (e) GeP_3@graphene, and (f) SnP_3@graphene. Yellow and blue colors indicate the positive and negative values of the electron.

0.2157*e*, which could significantly enhance the electric conductivity[53] and promote the[19] electrocatalytic activity. Hence, the electronic properties of monolayer MP_3 (M = Ge, Sn) can be effectively improved by attaching the monolayer to a graphene substrate.

The electron localization function (ELF) reflects the bonding nature in a system.[54] The covalent bonding in the monolayer GeP_3 and SnP_3 can be confirmed by the topological analysis of ELFs. As shown in Fig. 5(a)–(d), the ELF values of Ge–P, Sn–P and P–P bonds are all

higher than 0.85, suggesting that the valence electrons among adjacent atoms are shared, while the covalent bonds among Ge–P, Sn–P and P–P are formed. In the presence of an adsorbed hydrogen atom, the charge transfer from Ge to P results in a significant redistribution of charge density in the system, thereby rendering H adsorption. To explore the charge transfer behavior of GeP_3@graphene and SnP_3@graphene after the H adsorption, we computed the charge difference data by using Bader charge analysis codes.[55] The atomic charge difference is calculated by, $\Delta\rho = \rho_{total} - \rho_H - \rho_{MP3+graphene}$, where ρ_{total}, ρ_H and $\rho_{MP3+graphene}$ are the total charge density, the charge density of the isolated H atom, and the charge density of the MP_3@graphene (M = Ge, Sn), respectively. As shown in Fig. 5(e) and (f), the charge accumulation and depletion of the GeP_3 and SnP_3 are localized around the H–P bond, which indicates the charge transfer behavior mainly happens between the H and P atoms.

For a complete HER process, the first step is the hydrogen adsorption (Volmer reaction), and then followed by either a Heyrovsky ($H^* + H_3O^+ + e^- \rightarrow H_2 + H_2O$) or Tafel ($H^* + H^* \rightarrow H_2$) reaction.[56,57] A weak H bonding strength leads to a low Volmer reaction rate, whereas a strong bonding strength may result in a sluggish Heyrovsky or Tafel reaction kinetics. To better understand the reaction mechanism of HER on the GeP_3 and SnP_3 monolayers, both Heyrovsky and Tafel reactions are evaluated. As shown in Fig. 6(a), when the adsorbed H atom approaches the H atom of H_3O^+ in the surrounding water layer on the surface of GeP_3 monolayer, then the proton breaks away from the surface and forms a hydrogen molecule. The derived HER pathway of GeP_3 monolayer shows that an activation energy of 0.55 eV for the second-step Heyrovsky reaction under equilibrium potential. For the Tafel reaction, two adsorbed H atoms react to form H_2. The initial state shows a H–H distance of 3.39 Å on the surface of GeP_3 monolayer. The two H atoms then approach, and finally evolved H_2 molecule with an equilibrium H–H bond length of 0.75 Å on the GeP_3 monolayer surface. For this process the activation energy on GeP_3 surface is 0.14 eV. However, since the energy of final state is 0.88 eV higher than the initial state, the Tafel reaction path is less favorable than the Heyrovsky reaction. The similar trend of both Heyrovsky reaction (0.38 eV) and Tafel reaction (0.19 eV) on the SnP_3 surface is shown in Fig. 6(c) and (d), respectively. Therefore, the mechanism underneath the HER on

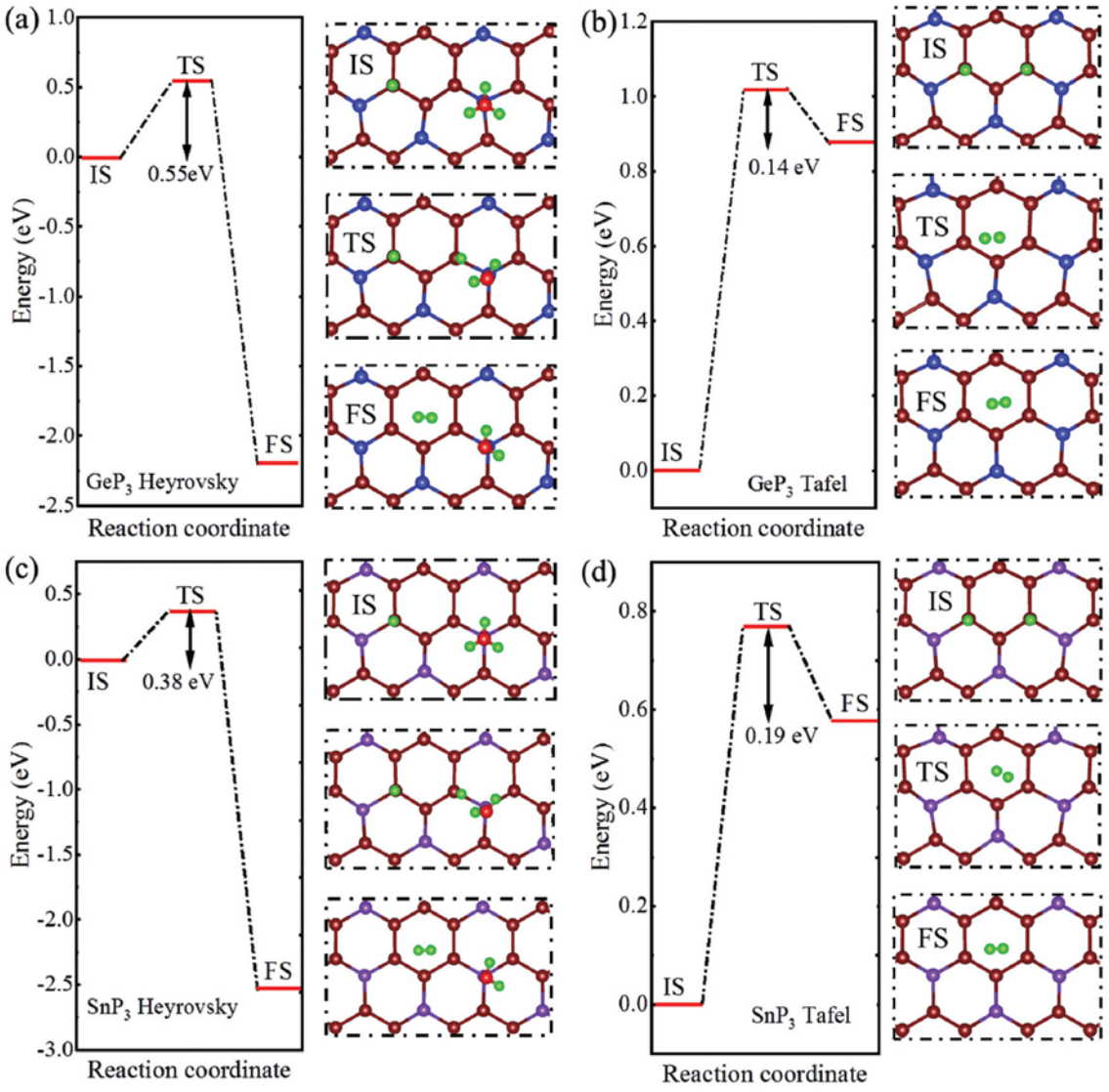

Fig. 6. Energy landscape for (a) Heyrovsky and (b) Tafel reaction on GeP_3 surface; (c) Heyrovsky and (d) Tafel reaction on SnP_3 surface. The right panel illustrate the reaction process including initial state (IS), transition state (TS) and final state (FS).

GeP_3 and SnP_3 type triphosphates monolayer should be a Heyrovsky-dominated Volmer–Heyrovsky reaction mechanism. Considering the HER performance may be pH-dependent due to different reaction pathways under alkaline and acidic conditions, [58] the suggested pH environment for the current study is acidic environment with the pH value equal zero.

4. Conclusions

In conclusion, by using density functional theory, we have systematically analyzed the GeP_3 and SnP_3 monolayers as potential electrocatalytic materials for HER. The calculation results demonstrate that GeP_3 is highly active for HER, with suitable adsorption free energy ΔG_{H^*} (0.024 eV) in the basal plane. The predicted high HER activity of GeP_3 is quite robust even with exerting external strain, suggesting that GeP_3 monolayer is better than Pt as an ideal catalyst for HER. The effect of graphene substrate is further assessed. It is found that the graphene substrate has a positive effect on the HER performance compared with that of a freestanding GeP_3 and SnP_3 monolayer, wherein charge transfer from GeP_3 and SnP_3 monolayer to graphene could significantly enhance the electronic conductivity and thus promote the electrocatalytic activity. The reaction kinetics reveal that the mechanism underneath the HER on GeP_3 and SnP_3 type triphosphate monolayers should be a Heyrovsky-dominated Volmer–Heyrovsky reaction process. This study suggests a new opportunity for the application of 2D triphosphates GeP_3 and SnP_3-based electrocatalysts and provide a new class of candidates for metal-free catalysts for HER.

Acknowledgments — QBZ was supported by the National Natural Science Foundation of China (Grants No. 21703185), the National Key Research Program of China (Grant No. 2016YFA0202602) and Fundamental Research Funds for the Central Universities (Xiamen University: 20720170042). The computational work was done on the computer facility in University of Nebraska Holland Computing Center. The authors appreciate fruitful discussions with Dr Jun Dai in the University of Nebraska-Lincoln.

Conflicts of interest — There are no conflicts to declare.

References

1 A. K. Geim and K. S. Novoselov, *Nat. Mater.*, 2007, 6, 183.

2 A. Fasolino, J. H. Los and M. I. Katsnelson, *Nat. Mater.*, 2007, 6, 858.

3 J. C. Meyer, A. K. Geim, M. I. Katsnelson, K. S. Novoselov, T. J. Booth and S. Roth, *Nature*, 2007, 446, 60.

4 C. R. Dean, A. F. Young, I. Meric, C. Lee, L. Wang, S. Sorgenfrei, K. Watanabe, T. Taniguchi, P. Kim and K. L. Shepard, *Nat. Nanotechnol.*, 2010, 5, 722.

5 F. Xia, H. Wang, D. Xiao, M. Dubey and A. Ramasubramaniam, *Nat. Photonics*, 2014, 8, 899.

6 L. Wang, I. Meric, P. Huang, Q. Gao, Y. Gao, H. Tran, T. Taniguchi, K. Watanabe, L. Campos and D. Muller, *Science*, 2013, 342, 614–617.

7 L. Li, E. O'Farrell, K. Loh, G. Eda, B. Özyilmaz and A. C. Neto, *Nature*, 2016, 529, 185.

8 Z. Wang, H.-H. Wu, Q. Li, F. Besenbacher, X. C. Zeng and M. Dong, *Nanoscale*, 2018, 10, 18178–18185.

9 H. Oughaddou, H. Enriquez, M. R. Tchalala, H. Yildirim, A. J. Mayne, A. Bendounan, G. Dujardin, M. A. Ali and A. Kara, *Prog. Surf. Sci.*, 2015, 90, 46–83.

10 A. Castellanos-Gomez, *J. Phys. Chem. Lett.*, 2015, 6, 4280–4291.

11 M. Naguib, *Adv. Mater.*, 2011, 23, 4248.

12 J. Zhou, J. Lin, X. Huang, Y. Zhou, Y. Chen, J. Xia, H. Wang, Y. Xie, H. Yu and J. Lei, *Nature*, 2018, 556, 355.

13 L. Li, Y. Yu, G. J. Ye, Q. Ge, X. Ou, H. Wu, D. Feng, X. H. Chen and Y. Zhang, *Nat. Nanotechnol.*, 2014, 9, 372.

14 B. Radisavljevic, A. Radenovic, J. Brivio, I. V. Giacometti and A. Kis, *Nat. Nanotechnol.*, 2011, 6, 147.

15 F. Zhang, C. Xia, J. Zhu, B. Ahmed, H. Liang, D. B. Velusamy, U. Schwingenschlögl and H. N. Alshareef, *Adv. Energy Mater.*, 2016, 6, 1601188.

16 J. S. Ross, P. Klement, A. M. Jones, N. J. Ghimire, J. Yan, D. Mandrus, T. Taniguchi, K. Watanabe, K. Kitamura and W. Yao, *Nat. Nanotechnol.*, 2014, 9, 268.

17 D. H. Cao, C. C. Stoumpos, O. K. Farha, J. T. Hupp and M. G. Kanatzidis, *J. Am. Chem. Soc.*, 2015, 137, 7843– 7850.

18 P. D. Tran, L. H. Wong, J. Barber and J. S. Loo, *Energy Environ. Sci.*, 2012, 5, 5902–5918.

19 J. Hong, C. Jin, J. Yuan and Z. Zhang, *Adv. Mater.*, 2017, 29, 1606434.

20 N. Lu, Z. Zhuo, H. Guo, P. Wu, W. Fa, X. Wu and X. C. Zeng, *J. Phys. Chem. Lett.*, 2018, 9, 1728–1733.

21 N. Miao, B. Xu, N. C. Bristowe, J. Zhou and Z. Sun, *J. Am. Chem. Soc.*, 2017, 139, 11125–11131.

22 S. Sun, F. Meng, H. Wang, H. Wang and Y. Ni, *J. Mater. Chem. A*, 2018, 6, 11890–11897.

23 Y. Jing, Y. Ma, Y. Li and T. Heine, *Nano Lett.*, 2017, 17, 1833–1838.

24 C. Zhang, Y. Jiao, T. He, F. Ma, L. Kou, T. Liao, S. Bottle and A. Du, *Phys. Chem. Chem. Phys.*, 2017, 19, 25886– 25890.

25 J. Liu, C.-S. Liu, X.-J. Ye and X.-H. Yan, *J. Mater. Chem. A*, 2018, 6, 3634–3641.

26 B. Ghosh, S. Puri, A. Agarwal and S. Bhowmick, *J. Phys. Chem. C*, 2018, 122, 18185–18191.

27 K. Maeda and K. Domen, *J. Phys. Chem. Lett.*, 2010, 1, 2655–2661.

28 J. K. Nørskov, T. Bligaard, A. Logadottir, J. Kitchin, J. G. Chen, S. Pandelov and U. Stimming, *J. Electrochem. Soc.*, 2005, 152, J23–J26.

29 B. Hinnemann, P. G. Moses, J. Bonde, K. P. Jørgensen, J. H. Nielsen, S. Horch, I. Chorkendorff and J. K. Nørskov, *J. Am. Chem. Soc.*, 2005, 127, 5308–5309.

30 G. Gao, Q. Sun and A. Du, *J. Phys. Chem. C*, 2016, 120, 16761–16766.

31 Z. Wang, Q. Li, H. Xu, C. Dahl-Petersen, Q. Yang, D. Cheng, D. Cao, F. Besenbacher, J. V. Lauritsen and S. Helveg, *Nano Energy*, 2018, 49, 634–643.

32 C. Tsai, F. Abild-Pedersen and J. K. Nørskov, *Nano Lett.*, 2014, 14, 1381–1387.

33 L. Shi, C. Ling, Y. Ouyang and J. Wang, *Nanoscale*, 2017, 9, 533–537.

34 C. Zhang, G. Yu, R. Ku, X. Huang and W. Chen, *Appl. Surf. Sci.*, 2019, 481, 272–280.

35 G. Kresse and J. Furthmüller, *Phys. Rev. B: Condens. Matter Mater. Phys.*, 1996, 54, 11169.

36 G. Kresse and D. Joubert, *Phys. Rev. B: Condens. Matter Mater. Phys.*, 1999, 59, 1758.

37 J. P. Perdew, *Phys. Rev. B: Condens. Matter Mater. Phys.*, 1992, 46, 6671.

38 J. Perdew and Y. Wang, *Phys. Rev. B*, 1992, 45, 13244.

39 H. Yang, H.-H. Wu, M. Ge, L. Li, Y. Yuan, Q. Yao, J. Chen, L. Xia, J. Zheng, Z. Chen, J. Duan, K. Kisslinger, X. C. Zeng, W.-K. Lee, Q. Zhang and J. Lu, *Adv. Funct. Mater.*, 2019, 29, 1808825.

40 L. Zhao, H.-H. Wu, C. Yang, Q. Zhang, G. Zhong, Z. Zheng, H. Chen, J. Wang, K. He, B. Wang, T. Zhu, X. C. Zeng, M. Liu and M.-S. Wang, *ACS Nano*, 2018, 12, 12597– 12611.

41 H. Huang, H.-H. Wu, C. Chi, B. Huang and T.-Y. Zhang, *J. Mater. Chem. A*, 2019, 7, 8897–8904.

42 S. Kümmel and L. Kronik, *Rev. Mod. Phys.*, 2008, 80, 3.

43 J. Heyd, J. E. Peralta, G. E. Scuseria and R. L. Martin, *J. Chem. Phys.*, 2005, 123, 174101.

44 J. Greeley, T. F. Jaramillo, J. Bonde, I. Chorkendorff and J. K. Nørskov, *Nat. Mater.*, 2006, 5, 909.

45 S. Yu, Y.-C. Rao, H.-H. Wu and X.-M. Duan, *Phys. Chem. Chem. Phys.*, 2018, 20, 27970–27974.

46 R. Chianelli, G. Berhault, P. Raybaud, S. Kasztelan, J. Hafner and H. Toulhoat, *Appl. Catal., A*, 2002, 227, 83–96.

47 O. Olofsson, *Acta Chem. Scand.*, 1970, 24, 1153–1162.

48 J. Gullman and O. Olofsson, *J. Solid State Chem.*, 1972, 5, 441–445.

49 P. Donohue and H. Young, *J. Solid State Chem.*, 1970, 1, 143–149.

50 H.-H. Wu, Q. Meng, H. Huang, C. Liu and X.-L. Wang, *Phys. Chem. Chem. Phys.*, 2018, 20, 3608–3613.

51 J. M. Bockris and E. Potter, *J. Electrochem. Soc.*, 1952, 99, 169–186.

52 Y. Shi and B. Zhang, *Chem. Soc. Rev.*, 2016, 45, 1529–1541.

53 D. Zou, S. Xie, Y. Liu, J. Lin and J. Li, *J. Mater. Chem. A*, 2013, 1, 8888–8896.

54 P.-L. Gong, F. Zhang, L.-F. Huang, H. Zhang, L. Li, R.-C. Xiao, B. Deng, H. Pan and X.-Q. Shi, *J. Phys.: Condens. Matter*, 2018, 30, 475702.

55 W. Tang, E. Sanville and G. Henkelman, *J. Phys.: Condens. Matter*, 2009, 21, 084204.

56 L. X. Chen, Z. W. Chen, Y. Wang, C. C. Yang and Q. Jiang, *ACS Catal.*, 2018, 8, 8107–8114.

57 X. Lv, W. Wei, H. Wang, B. Huang and Y. Dai, *Appl. Catal., B*, 2019, 255, 117743.

58 J. Liu, Y. Zheng, D. Zhu, A. Vasileff, T. Ling and S.-Z. Qiao, *Nanoscale*, 2017, 9, 16616–16621.

Supplementary information follows.

Electronic Supplementary Information

Monolayer triphosphates MP_3 (M=Sn, Ge) with excellent basal catalytic activity for hydrogen evolution reaction

Hong-Hui Wu[‡], He Huang[§], Jie Zhong[‡], Song Yu[∇], Qiaobao Zhang[†]*, Xiao Cheng Zeng [‡]*

[†] Department of Materials Science and Engineering, College of Materials, Xiamen University, Xiamen, Fujian 361005, China.

[‡] Department of Chemistry, University of Nebraska-Lincoln, NE 8588 Lincoln, United States

[§] Department of Mechanical and Aerospace Engineering, Hong Kong University of Science and Technology, Clear Water Bay, Kowloon, Hong Kong, China.

[∇] Department of Physics and Materials, East China Normal University, Shanghai 200241, China

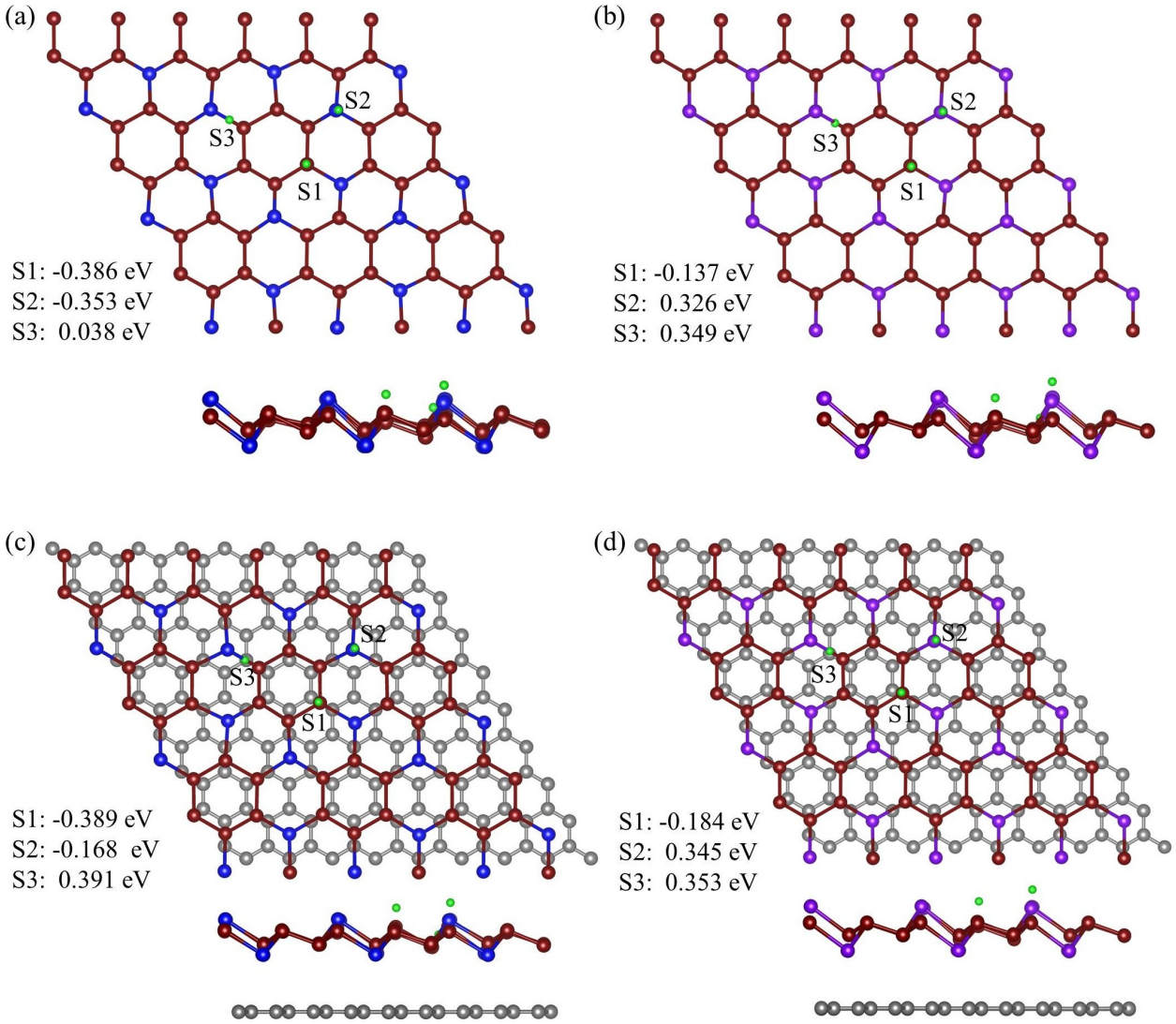

Figure S1. Top and side view of the optimized structural 4×4×1 supercell of (a) GeP_3 monolayer, (b) SnP_3 monolayer, (c) GeP_3@graphene, (d) SnP_3@graphene.

Table S1 Computed bond length, monolayer thickness and layer distance for GeP_3 and SnP_3

System	Ge (Sn)-P	P-P	P-H	thickness	layer distance
GeP_3	2.508	2.175	1.432	2.421	/
SnP_3	2.712	2.168	1.434	2.875	/
GeP_3@graphene	2.566	2.211	1.435	5.239	3.208
SnP3@graphene	2.731	2.184	1.435	5.921	3.338

Table S2. Computed adsorption energy (E_a), adsorption distance (*d*), charge transfer (ΔQ) of the atoms around the adsorption site

System	E_a (eV)	*d* (Å)	Bader charge of hydrogen atom	ΔQ (e)
GeP_3	-0.386	1.431	1.319	0.319
GeP_3@graphene	-0.389	1.434	1.351	0.351
SnP_3	-0.137	1.433	1.312	0.312
SnP_3@graphene	-0.185	1.434	1.379	0.379

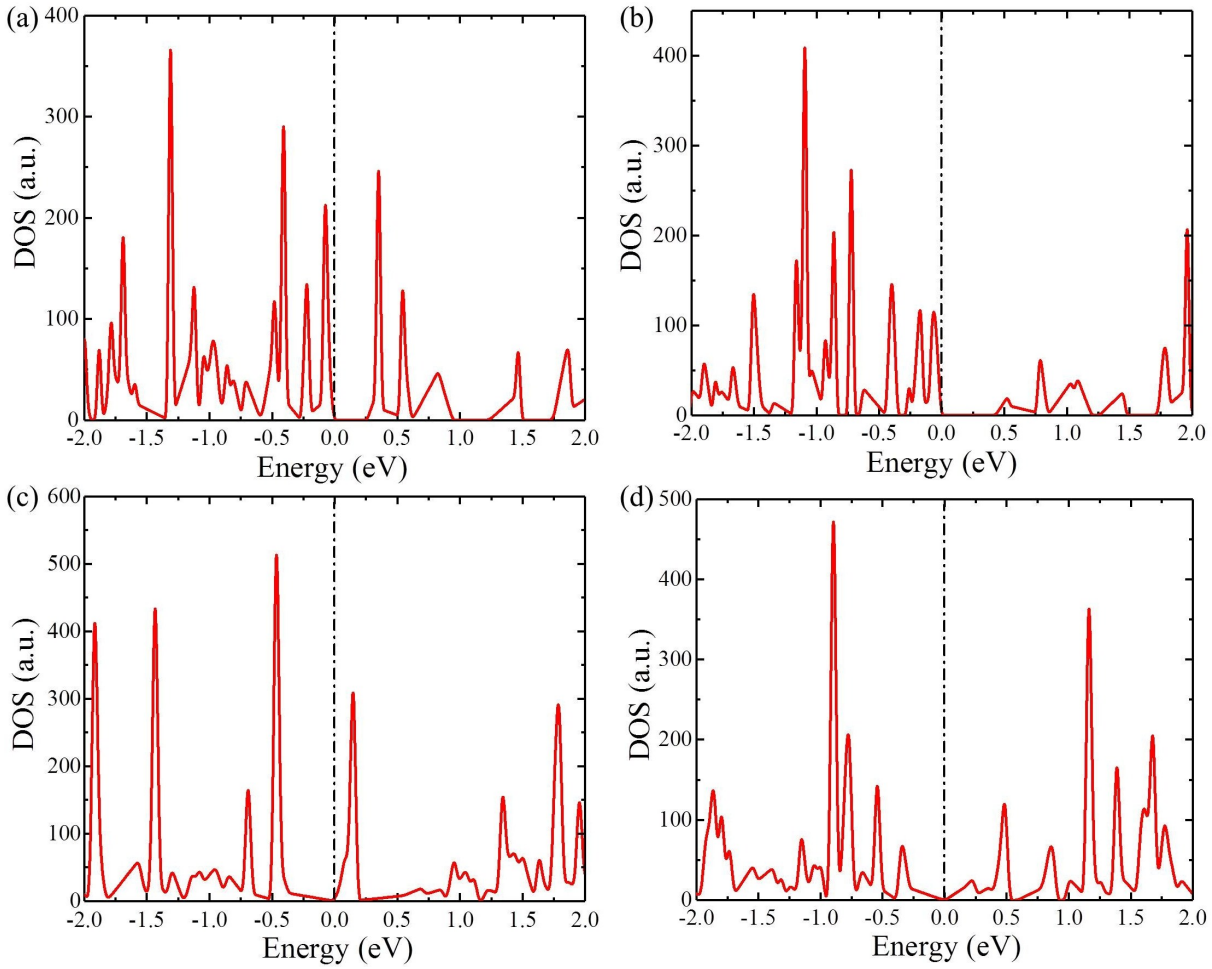

Figure S2. Density of states computed based on the PBE functional for (a) GeP_3 monolayer, (b) SnP_3 monolayer, (c) GeP_3@graphene heterobilayer, and (d) SnP_3@graphene heterobilayer.

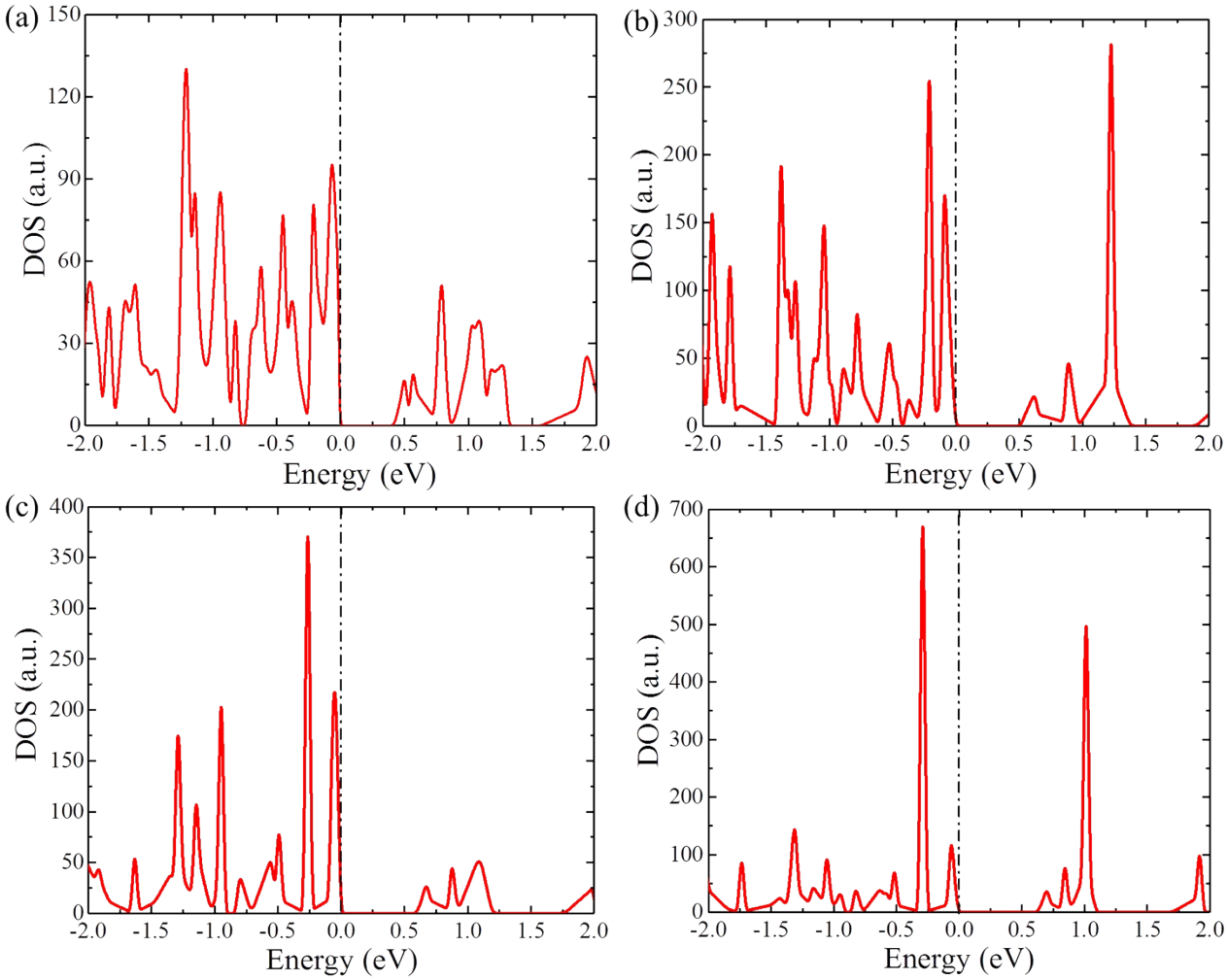

Figure S3. Effect of biaxial strain (a) -0.02, (b) -0.01, (c) 0.01, (d) 0.02 on the density of states of GeP_3 monolayer, based on HSE06 computation.

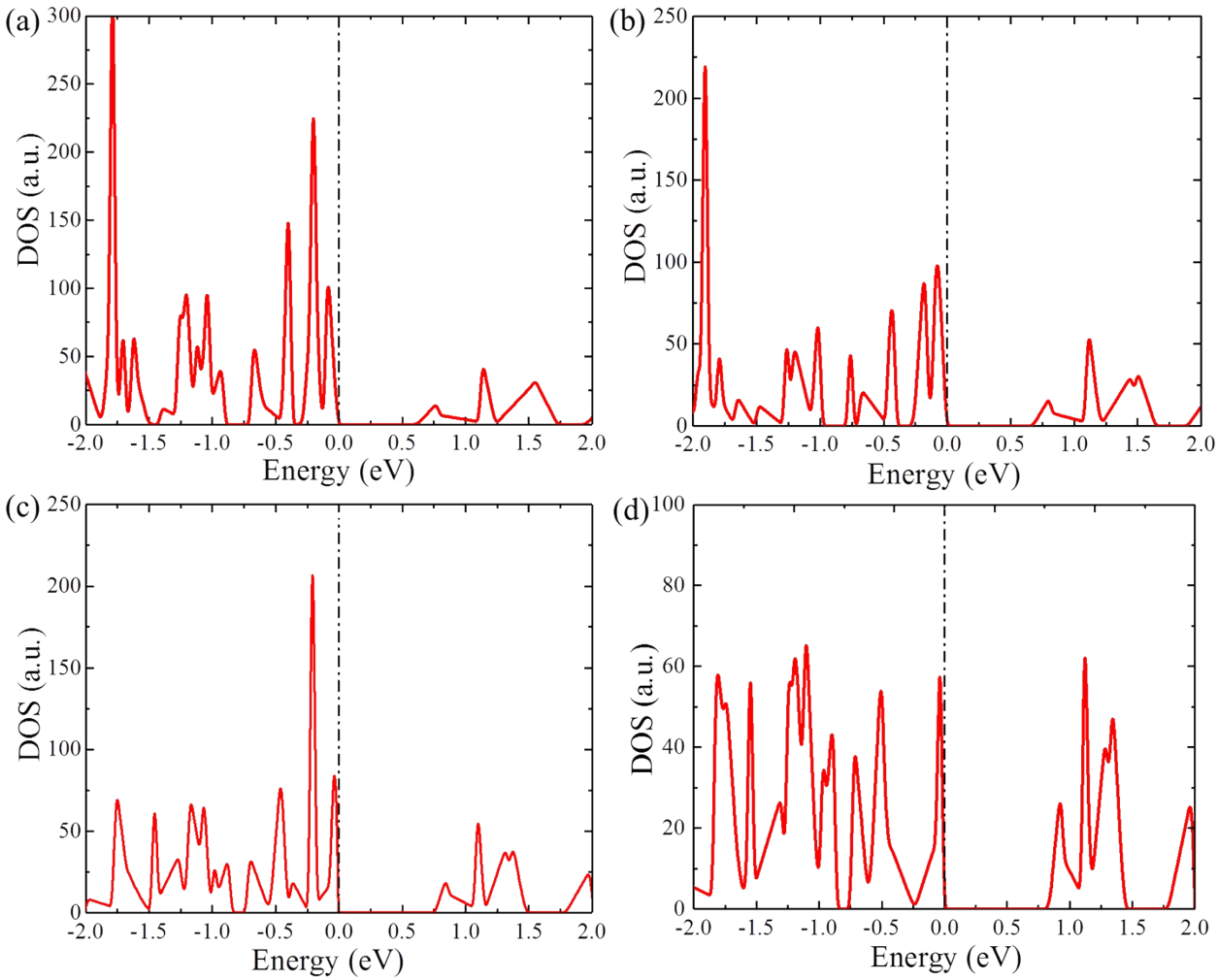

Figure S4. Effect of biaxial strain (a) -0.02, (b) -0.01, (c) 0.01, (d) 0.02 on the density of states of SnP_3 monolayer, based on HSE06 computation.

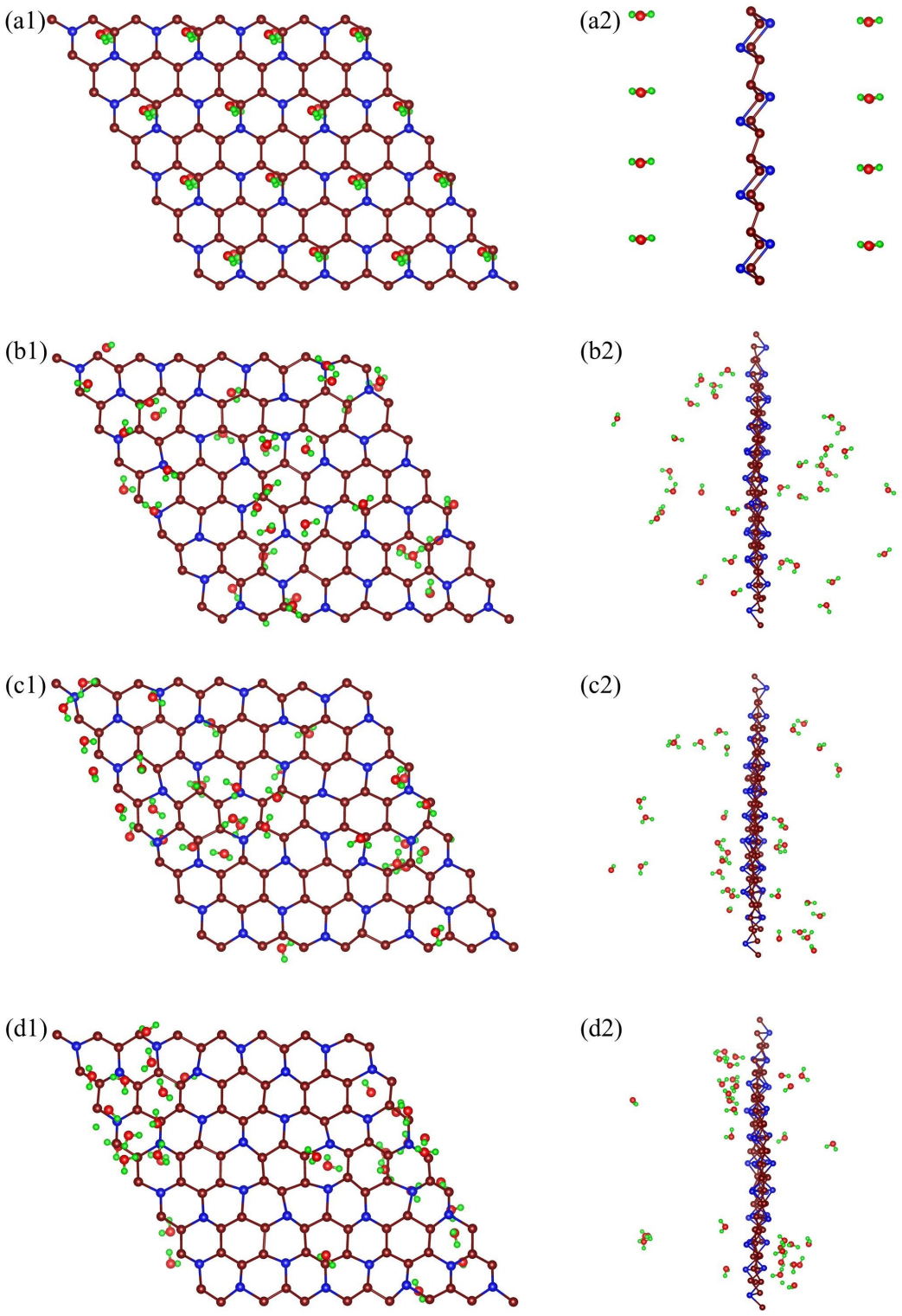

Figure S5. Ab initio MD simulation results of the 6×6×1 GeP_3 monolayer supercell with 32 water molecules at the simulation time (a1)-(a2) 0 fs, (b1)-(b2) 1000 fs, (c1)-(c2) 3000 fs, (d1)-(d2) 6000 fs from top and side view, respectively. The temperature is controlled at 300 K.

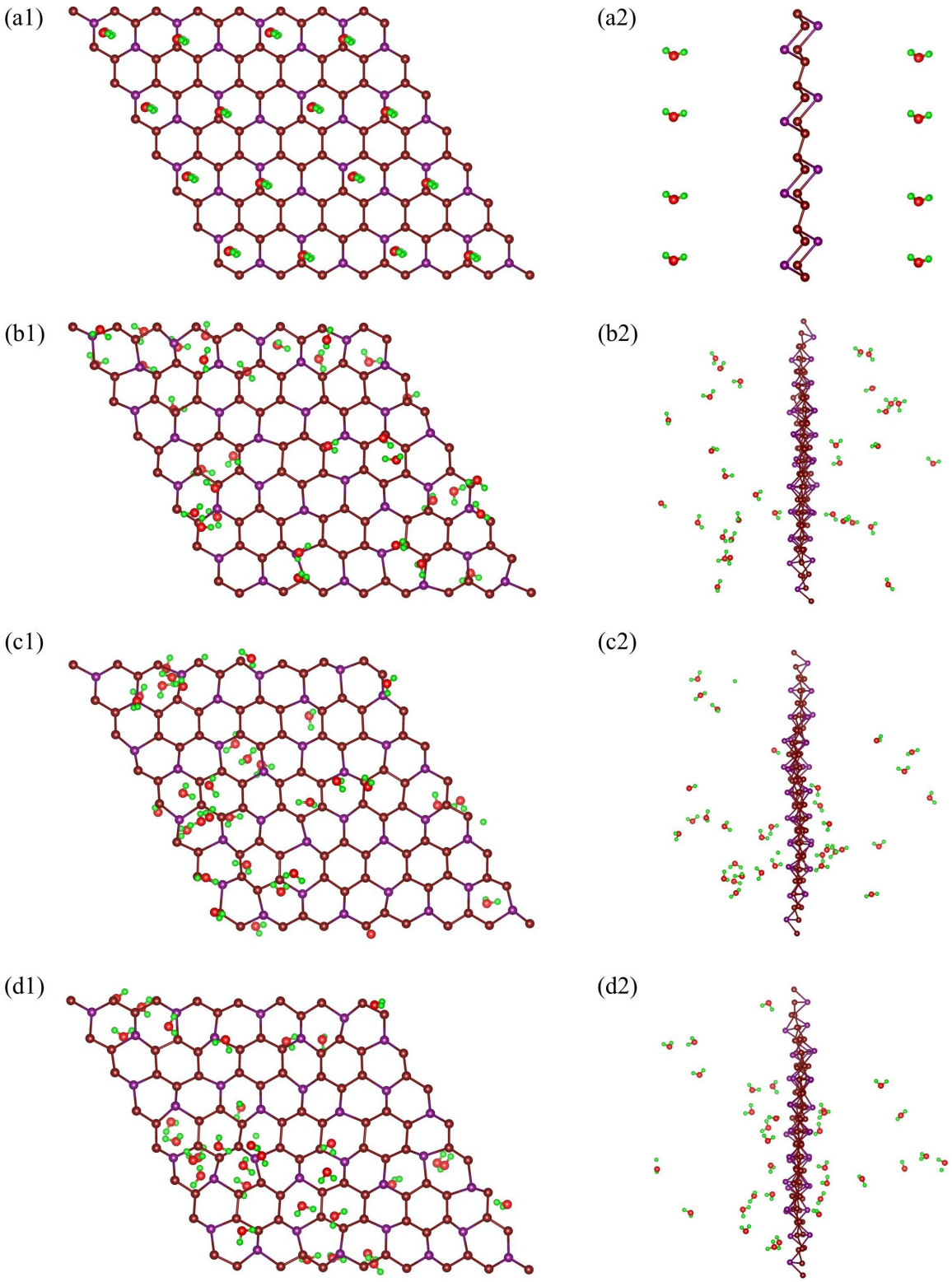

Figure S6. Ab initio MD simulation results of the 6×6×1 SnP_3 monolayer supercell with 32 water molecules at the simulation time (a1)-(a2) 0 fs, (b1)-(b2) 1000 fs, (c1)-(c2) 3000 fs, (d1)-(d2) 6000 fs from top and side view, respectively. The temperature is controlled at 300 K.